ELSEVIER

Journal of Nuclear Materials 289 (2001) 188–193

journal of nuclear materials

www.elsevier.nl/locate/jnucmat

Heavy-ion irradiation effects in $Gd_2(Ti_{2-x}Zr_x)O_7$ pyrochlores

B.D. Begg [a,*], N.J. Hess [b], D.E. McCready [b], S. Thevuthasan [b], W.J. Weber [b]

[a] *Materials Division, Australian Nuclear Science and Technology Organisation, PMB1, Menai NSW 2234, Australia*
[b] *Pacific Northwest National Laboratory, Richland, WA 99352, USA*

Abstract

$Gd_2(Ti_{2-x}Zr_x)O_7$ samples with $0 \leqslant x \leqslant 1.5$ were single-phase and pyrochlore structured after sintering at 1600°C in air. The $Gd_2Zr_2O_7$ ($x = 2$) end member predominantly displayed an anion deficient-fluorite structure. Raman spectroscopy indicated that the level of short-range fluorite-like disorder in the unirradiated $Gd_2(Ti_{2-x}Zr_x)O_7$ samples increased significantly as Zr was substituted for Ti, despite the retention of a long-range pyrochlore structure for samples with $0 \leqslant x \leqslant 1.5$. Glancing-incidence X-ray diffraction indicated that pyrochlores with an ionic radii ratio $r_A/r_B \leqslant 1.52 (x \geqslant 1.5)$ were transformed into a radiation resistant defect-fluorite structure after irradiation at room temperature with 2 MeV Au^{2+} to a fluence of 5 ions/nm^2. As the ionic radii ratio of the pyrochlore increased beyond $r_A/r_B > 1.52$, the defect-fluorite structure became increasingly unstable with respect to the amorphous state under identical irradiation conditions.

1. Introduction

Pyrochlore is one of a number of candidate materials proposed for the immobilisation of actinide-rich wastes, and has recently been selected as a key component in the synroc-based pyrochlore-rich ceramics for the geological immobilisation of surplus Pu in the US. The pyrochlores under consideration typically exhibit $A_2B_2O_7$ stoichiometry, where actinides and lanthanides are incorporated on the eight-coordinate A-site and either Ti or Zr occupy the six-coordinate B-site. The pyrochlore structure is derived from a fluorite sub-cell, with twice the lattice parameter, two cation sites and one-eighth fewer anions. Pyrochlores can accommodate a wide variety of chemical substitutions, provided charge neutrality and certain ionic size criteria are satisfied. The stability of the $A_2^{3+}B_2^{4+}O_7$ pyrochlores is governed by the ionic radii ratio of the A and B site cations (r_A/r_B). For pyrochlores prepared at atmospheric pressure and temperatures up to 1500°C, the range of pyrochlore stability extends from $r_A/r_B = 1.46$ for $Gd_2Zr_2O_7$ to $r_A/r_B = 1.78$ for $Sm_2Ti_2O_7$. For smaller ionic radii ratios, $r_A/r_B < 1.46$, anion-deficient fluorite is the stable structure, whilst the monoclinic structure is stable for ionic radii ratios $r_A/r_B > 1.78$ [1].

Given that actinide-bearing crystalline waste forms will be subject to considerable α-recoil radiation damage it is important to understand the effect of radiation damage on the pyrochlore structure. Considerable work has been carried out characterising the irradiation induced crystalline-to-amorphous transformation observed in titanate-based pyrochlores [2–4]. More recently, pyrochlores of $Gd_2(Ti_{2-x}Zr_x)O_7$ stoichiometry have been investigated which display a systematic decrease in susceptibility to radiation induced amorphisation with increasing Zr content [5]. The end member $Gd_2Zr_2O_7$ was totally resistant to amorphisation even at 25 K [5,6].

This paper presents detailed characterisation of the as-prepared crystalline $Gd_2(Ti_{2-x}Zr_x)O_7$ family of pyrochlores for $x = 0, 0.5, 1, 1.5$ and 2, whose ionic radii ratios span the complete pyrochlore stability field from $r_A/r_B = 1.74$ ($x = 0$) to $r_A/r_B = 1.46$ ($x = 2$), along with characterisation of the structural changes associated with irradiation with 2 MeV Au^{2+} to a fluence of 5 ions/nm^2.

2. Experimental

All samples were prepared via an alkoxide route from a liquid mixture of titanium iso-propoxide, tetra-butyl

* Corresponding author. Tel.: +61-2 9717 3747; fax: +61-2 9543 7179.
E-mail address: bruce.begg@ansto.gov.au (B.D. Begg).

0022-3115/01/$ - see front matter
PII: S0022-3115(00)00696-6

zirconate and gadolinium nitrate. These solutions were stir-dried and calcined at 700°C for 1 h in air. The calcine was then dried, ball-milled and then wet ball-milled before being pressed into pellets and sintered at 1600°C for 50 h in air. The sintered pellets were polished to a 0.5 μm diamond finish, and irradiated at room temperature with 2 MeV Au^{2+} ions to a fluence of 5 ions/nm^2 using the accelerator facilities within the Environmental Molecular Sciences Laboratory at PNNL [7].

Glancing-incidence X-ray diffraction (XRD) was carried out on a Philips PW3040/00 X'Pert MPD diffractometer using Cu Kα radiation. A variable slit was used to keep the irradiated area constant as 2θ varied, for each glancing angle. Integrated peak intensities were measured by fitting the diffraction peaks with pseudo-Voigt profiles, once the background had been subtracted with a cubic spline. Scanning electron-microscopy (SEM) was performed on a LEO 982 Field Emission instrument operating at 20 kV. Compositional analyses were obtained using an Oxford ISIS energy dispersive spectrometer.

Polarized Raman spectra were measured with a 1 mm spot size using approximately 500 mW of 488.0 nm excitation from a CW Argon ion laser. The Raman scattered light was scrambled prior to being focused on the entrance slit of a SPEX triple spectrometer. The exit slit was maintained at 75 μm and the scattered light was then dispersed on to a liquid nitrogen cooled charged coupled device Ge detector. The detector was calibrated using the Raman lines of a TiO_2 (anatase) standard. The Raman signal was collected for 60 s for all samples. The Raman spectra were analysed using a commercially available software package, GRAM.

3. Results

3.1. Unirradiated $Gd_2(Ti_{2-x}Zr_x)O_7$, $x = 0, 0.5, 1, 1.5, 2$

3.1.1. Scanning-electron microscopy

Scanning-electron microscopy of the sintered pyrochlores revealed that they were all homogeneous and single-phase. The results of the compositional analysis are shown in Table 1 and are accurate to approximately ±0.02 formula units.

3.1.2. X-ray diffraction

Characterisation of the long-range structure of these $Gd_2(Ti_{2-x}Zr_x)O_7$ samples was carried out using X-ray diffraction. Samples with $0 \leqslant x \leqslant 1.5$ were found to be pyrochlore structured, and exhibited a systematic increase in lattice parameter as the level of Zr substituting for Ti increased, as shown in Fig. 1. This lattice expansion results from Zr having a larger ionic radii, 0.072 nm (six coordinate) than Ti, 0.0605 nm (six coordinate). In contrast, the $x = 2$ sample was found to be predominantly defect-fluorite structured, although it did retain a small portion of pyrochlore. As mentioned earlier fluorite and pyrochlore are closely related cubic structures, although fluorite has a unit cell lattice parameter that is half that of pyrochlore, which accounts for the significant drop in lattice parameter for the $x = 2$ sample shown in Fig. 1.

Whilst $Gd_2Zr_2O_7$ ($x = 2$) with its ionic radii ratio, $r_A/r_B = 1.46$, resides on the edge of the pyrochlore stability field at 1500°C, it is known to undergo a pyrochlore-to-fluorite (order–disorder) transition when heated above 1530°C [1]. The predominance of a defect-fluorite in this sample therefore was not surprising, as it was sintered at 1600°C, well above this order–disorder transition temperature and the transformation from fluorite back to pyrochlore is very slow, even at high temperatures just below the order–disorder transformation temperature [8]. There was no evidence for any defect-fluorite structured material in the $x = 1.5$ sample.

3.1.3. Raman spectroscopy

The crystalline $Gd_2(Ti_{2-x}Zr_x)O_7$ samples ($x = 0, 0.5, 1, 1.5$ and 2) were also examined by Raman spectroscopy

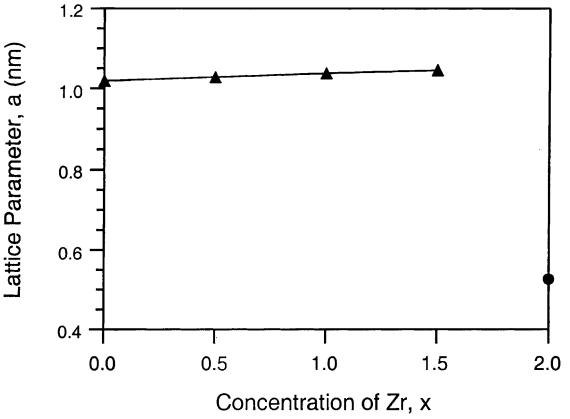

Fig. 1. Lattice parameters of the $Gd_2(Ti_{2-x}Zr_x)O_7$ as a function of increasing Zr content, x.

Table 1
Summary of the microanalysis results from each of the $Gd_2(Ti_{2-x}Zr_x)O_7$ pyrochlores

$Gd_2(Ti_{2-x}Zr_x)O_7$				
$x = 0$	$x = 0.5$	$x = 1.0$	$x = 1.5$	$x = 2$
$Gd_{2.02}Ti_{1.97}O_7$	$Gd_{2.03}Ti_{1.51}Zr_{0.47}O_7$	$Gd_{2.07}Ti_{1.01}Zr_{0.93}O_7$	$Gd_{2.06}Ti_{0.51}Zr_{1.44}O_7$	$Gd_{2.00}Zr_{2.00}O_7$

to look for short-range structural differences across the $Gd_2Ti_2O_7$–$Gd_2Zr_2O_7$ tie line. The Raman spectra from the $Gd_2(Ti_{2-x}Zr_x)O_7$ pyrochlores, shown in Fig. 2, are dominated by two intense bands at ~310 cm^{-1} and ~512 cm^{-1}, which have been previously assigned to the O–Gd–O bending and Gd–O stretching modes, respectively, [8]. The most notable difference in the Raman spectra between the various samples is the significant increase in full-width-at-half-maximum intensity (FWHM) of the O–Gd–O bending and Gd–O stretching modes as the level of Zr substituting for Ti increases. The Raman intensities of these O–Gd–O bending and Gd–O stretching modes are also significantly reduced in the samples with $x \geqslant 1$ in the lead up to the long-range structural transition to the anion deficient-fluorite observed at $x = 2$. The Raman shift of the Ti–O stretching mode at approximately 450 cm^{-1} in the $x = 0$ sample also contracts to smaller wave numbers as Ti is systematically replaced by Zr, as indicated in Fig. 2.

The significant broadening of all the vibrational modes indicates that the level of localised short-range disorder is increasing as Zr is substituted for Ti in $Gd_2(Ti_{2-x}Zr_x)O_7$. Significantly in the pyrochlore-structured samples, $0 \leqslant x \leqslant 1.5$, the effect of this substitution is clearly evident in the vibrational modes associated with the Gd site. This would suggest that despite their long-range pyrochlore structure, the short-range structure exhibits increasing levels of localised cation site mixing or fluorite-like disorder.

3.2. 2 MeV Au^{2+} irradiations

A sample from each $Gd_2(Ti_{2-x}Zr_x)O_7$ ($x = 0, 0.5, 1, 1.5$ and 2) composition was irradiated at room temperature with 2 MeV Au^{2+} to an ion fluence of 5 ions/nm^2. TRIM calculations for $Gd_2Ti_2O_7$ ($x = 0$), using a displacement energy of 50 eV, suggests that this would be sufficient to achieve the fully amorphous state to a depth of 380 nm based on previous results [2–6]. The structure of these irradiated samples was examined by glancing-incidence XRD, using a range of glancing angles from 1° to 10° to characterise the structure as a function of depth. This is possible since the X-ray penetration depth is proportional to the glancing-angle of the incident X-ray beam. Consequently X-ray diffraction patterns obtained a low glancing angles are very surface sensitive, whilst those obtained at large glancing-angles are more bulk sensitive.

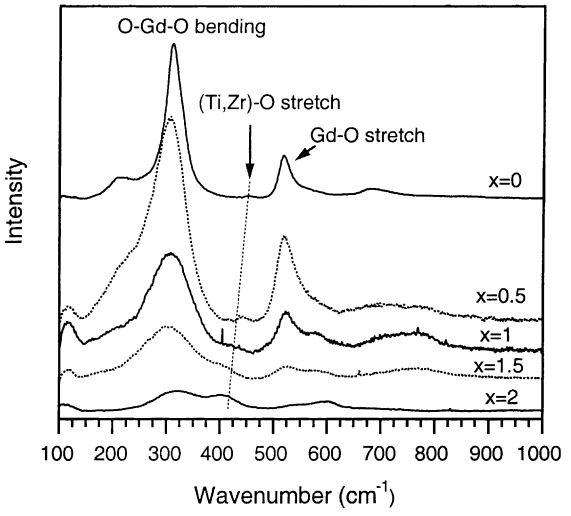

Fig. 2. Raman spectra from unirradiated $Gd_2(Ti_{2-x}Zr_x)O_7$ samples for $x = 0, 0.5, 1, 1.5$ and 2.

3.3. $Gd_2Zr_2O_7$, ($x = 2$)

The small proportion of pyrochlore present in the as-prepared sample was readily transformed to a defect-fluorite structure as a result of this irradiation treatment (see Fig. 3). The diffraction pattern obtained with a 10° glancing angle, which samples the substrate beyond the reach of the ion beam, shows a number of unique pyrochlore peaks which are clearly absent in the near-surface irradiated region. In this instance the 2 MeV Au^{2+} ion fluence of 5 ions/nm^2 served merely to complete the cation disordering, required for the pyrochlore-to-fluorite transformation, that was already well advanced after sintering this material at 1600°C for 50 h. Consistent with previous results at much higher equivalent doses [5,6], the defect-fluorite structured material showed no evidence of amorphisation.

3.4. $Gd_2Ti_{0.5}Zr_{1.5}O_7$, ($x = 1.5$)

Fig. 4 shows a selection of glancing-incidence diffraction patterns obtained from $Gd_2Ti_{0.5}Zr_{1.5}O_7$ after

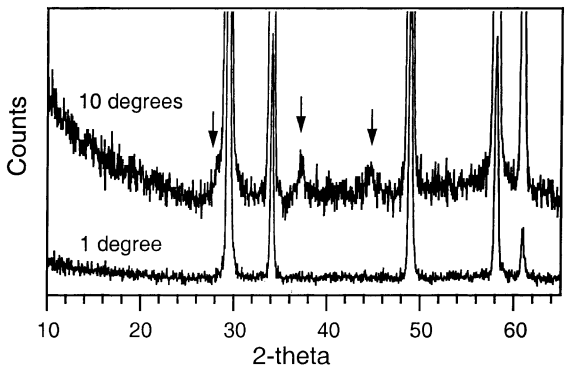

Fig. 3. Glancing-incidence X-ray diffraction patterns from $Gd_2Zr_2O_7$ irradiated with 2 MeV Au^{2+} to a fluence of 5 Au^+/nm^2. The positions of the unique pyrochlore peaks have been marked with an arrow.

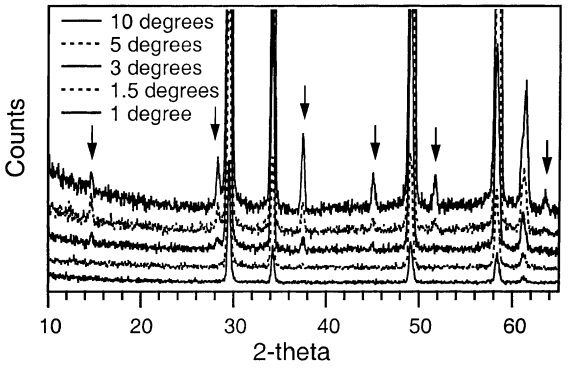

Fig. 4. Glancing-incidence X-ray diffraction patterns from $Gd_2Ti_{0.5}Zr_{1.5}O_7$ irradiated with 2 MeV Au^{2+} to a fluence of 5 Au^+/nm^2. The positions of the unique pyrochlore peaks have been marked with an arrow. The diffraction patterns have been offset for clarity and are in the same order as the legend.

irradiating with 2 MeV Au^{2+} to an ion fluence of 5 ions/nm^2. Data obtained at glancing angles up to 1.5° indicate that the structure of the surface layer had been fully transformed to an anion deficient-fluorite, as a result of this irradiation treatment. No diffuse scattering was evident around any of the Bragg peaks that would indicate the presence of disorder in the defect-fluorite structured lattice. As glancing angles increase beyond 1.5°, ordered pyrochlore peaks develop as the X-rays begin to penetrate through to the unirradiated substrate.

Despite being initially pyrochlore-structured and having an ionic radii ratio of r_A/r_B of 1.52 defect fluorite-structured $Gd_2Ti_{0.5}Zr_{1.5}O_7$ ($x = 1.5$) has been stabilised without amorphisation after irradiation with 2 MeV Au^{2+} to an ion fluence of 5 ions/nm^2. The resistance of this composition to amorphisation is consistent with previous in situ TEM observations at much higher dose [5]. Whilst in this instance the driving force for this pyrochlore-to-fluorite (order–disorder) transformation has been cation disordering via ion-beam irradiation, this transformation can be induced in other zirconate pyrochlores whose ionic radii ratios span that of $Gd_2Ti_{0.5}Zr_{1.5}O_7$, namely $Sm_2Zr_2O_7$ (r_A/r_B of 1.50) and $Nd_2Zr_2O_7$ (r_A/r_B of 1.54) by heating above 2000°C and 2300°C, respectively, [1]. Therefore whilst these zirconate pyrochlores with an ionic radii ratio from r_A/r_B of between 1.50 and 1.54 normally exist well inside the pyrochlore stability field, if a driving force for cation disordering exists, such as high-temperature annealing or ion-beam irradiation, they readily undergo an order–disorder pyrochlore-to-fluorite transformation. The readiness with which this pyrochlore transforms to an anion-deficient fluorite structure is consistent with the earlier Raman results on the unirradiated $Gd_2Ti_{0.5}Zr_{1.5}O_7$ sample that indicated that it contained a high-level of short-range fluorite-like disorder despite its long-range pyrochlore structure.

3.5. Gd_2TiZrO_7, ($x = 1.0$)

In contrast to the previous samples, irradiating Gd_2TiZrO_7 with 2 MeV Au^{2+} to an ion fluence of 5 ions/nm^2 was sufficient to render a portion of the sample amorphous, in agreement with previous in situ TEM observations [5]. Significantly the surface layer of the sample appears to be crystalline, with no evidence of diffuse scattering in the diffraction pattern taken at the narrowest glancing angle of 1°, see Fig. 5. Whilst the signal-to-noise ratio of the data at low glancing angles is not optimum, the crystalline surface layer appears to be fluorite-structured consisting of the halved 111, 220 and 311 peaks, with respect to pyrochlore, in patterns obtained at 1° and 1.5°. The pattern obtained at 1.5° also contains the 200 fluorite peak (400 in pyrochlore). The presence of buried amorphous material, most easily seen in the diffuse scattering around the base of the 222 pyrochlore peak, becomes apparent at glancing angles of 1.5° and above, whilst the unique pyrochlore peaks are seen at glancing angles from 2° up. More detailed diffraction work is required to confirm this structural progression, which could potentially cast light on the amorphisation process. Further work is also being conducted on Gd_2TiZrO_7 irradiated to lower ion fluences.

Clearly the Gd_2TiZrO_7 sample, with its ionic radii ratio of $r_A/r_B = 1.59$, has exceeded the defect-fluorite structural stability limit under these irradiation conditions, resulting in the formation of a buried amorphous layer. Significantly pyrochlore-structured $La_2Zr_2O_7$ which has an ionic radii ratio of $r_A/r_B = 1.61$, slightly larger than that of Gd_2TiZrO_7, also cannot be transformed to a defect-fluorite structure via high-temperature annealing [1]. Therefore it would appear that the maximum zirconate pyrochlore ionic radii ratio that is still capable of being transformed into a stable anion-deficient fluorite structure lies between $r_A/r_B = 1.54$ ($Nd_2Zr_2O_7$ [1]) and $r_A/r_B = 1.59$ (Gd_2TiZrO_7). Further work is being conducted to determine whether defect-fluorite structured Gd_2TiZrO_7 may be stabilised in the absence of any amorphous material under less severe irradiation conditions.

3.6. $Gd_2Ti_{1.5}Zr_{0.5}O_7$, ($x = 0.5$)

Parallel irradiation of the $Gd_2Ti_{1.5}Zr_{0.5}O_7$ pyrochlore rendered a significant fraction of this material amorphous, as shown in Fig. 6. In this instance, significant diffuse scattering, in the absence of any crystalline peaks, was present in the diffraction pattern collected at the narrowest 1° glancing angle, indicating that the surface had been fully amorphised. Crystalline peaks appeared

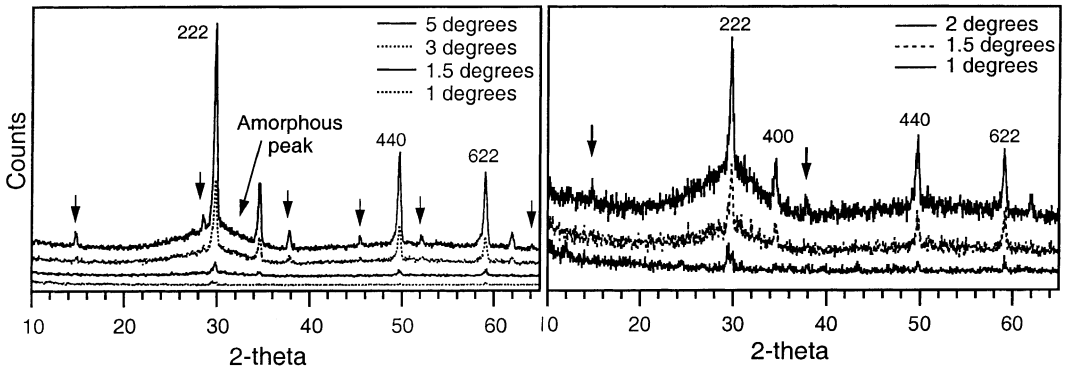

Fig. 5. Glancing-incidence X-ray diffraction patterns from Gd_2TiZrO_7 irradiated with 2 MeV Au^{2+} to a fluence of 5 Au^+/nm^2. The positions of the unique pyrochlore peaks have been marked with an arrow. The figure on the right shows an expanded view of the low angle patterns. The diffraction patterns have been offset for clarity and are in the same order as the legend.

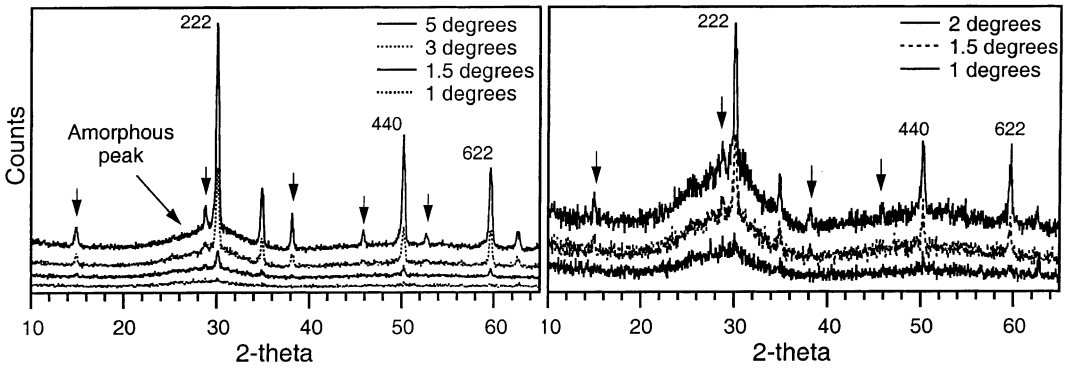

Fig. 6. Glancing-incidence X-ray diffraction patterns from $Gd_2Ti_{1.5}Zr_{0.5}O_7$ irradiated with 5 Au^+/nm^2. The positions of the unique pyrochlore peaks have been marked with an arrow. The figure on the right shows an expanded view of the low angle patterns. The diffraction patterns have been offset for clarity and are in the same order as the legend.

in the diffraction pattern collected at 1.5°, and were pyrochlore structured. There was no evidence of a sub-surface fluorite-structured layer either in conjunction with or just beyond the amorphous surface layer. The failure to observe any anion-deficient fluorite structured material suggests that the large ionic radii ratio of $Gd_2Ti_{1.5}Zr_{0.5}O_7(r_A/r_B = 1.66)$ places this pyrochlore in a region where the defect-fluorite structure is very unstable with respect to the amorphous state under these irradiation conditions.

3.7. $Gd_2Ti_2O_7$, $(x = 0)$

The effects of 2 MeV Au^{2+} irradiations on the structure of $Gd_2Ti_2O_7$ to a variety of ion fluences have been reported previously [9]. Irradiating $Gd_2Ti_2O_7$ to a slightly lower fluence of 3 ions/nm^2 resulted in the complete amorphisation of the surface to a depth of ~340 nm. No evidence of any defect-fluorite structured material was seen in this sample, in fact defect-fluorite was only observed, in conjunction with pyrochlore, at very low ion fluences of ~0.3 ions/nm^2, which reflects its diminishing stability with reflect to the amorphous state. $Gd_2Ti_2O_7$ has a very large ionic radii ratio of $r_A/r_B = 1.74$, which approaches the opposing border of the pyrochlore-monoclinic phase field $r_A/r_B = 1.78$ (for $Sm_2Ti_2O_7$), and consequently the stability of the irradiation-induced defect-fluorite structure is very minimal.

4. Conclusions

$Gd_2(Ti_{2-x}Zr_x)O_7$ samples with $0 \leqslant x \leqslant 1.5$ were single-phase and pyrochlore structured after sintering at 1600°C. The $Gd_2Zr_2O_7$ $(x = 2)$ end member adopted a predominantly anion deficient-fluorite structure. Raman spectroscopy indicated that the level of short-range fluorite-like disorder in the unirradiated $Gd_2(Ti_{2-x}Zr_x)O_7$ samples increased significantly as Zr was substituted for Ti, despite the retention of a long-range pyrochlore

structure for samples with $0 \leqslant x \leqslant 1.5$. Pyrochlores with an ionic radii ratio less than $r_A/r_B \leqslant 1.52 (x \geqslant 1.5)$ were transformed into a stable radiation resistant defect-fluorite structure after irradiation with 2 Mev Au^{2+} to a fluence of 5 ions/nm^2. As the ionic radii ratio of the pyrochlore increased beyond $r_A/r_B > 1.52$ ($x < 1.5$), the defect-fluorite structure became increasing unstable with respect to the amorphous state. A defect-fluorite structured surface layer was observed over a buried amorphous layer in the irradiated $x = 1$ sample ($r_A/r_B = 1.59$). No fluorite-structured material was observed in the similarly irradiated $x = 0.5$ or $x = 0$ samples ($r_A/r_B \geqslant 1.66$).

Acknowledgements

This research was a collaborative effort supported by the Australian Nuclear Science and Technology Organisation and the Division of Materials Sciences, Office of Basic Energy Sciences, U.S. Department of Energy. The experiments were performed at the EMSL, a national scientific user facility located at PNNL and supported by the U.S. Department of Energy's, Office of Biological and Environmental Research. PNNL is a multi-program national laboratory operated for the U.S. DOE by Battelle Memorial Institute under contract No. DE-AC06-76RLO 1830.

References

[1] M.A. Subramanian, G. Aravamudan, G.V. Subba Rao, Prog. Solid State Chem. 15 (1983) 55.
[2] W.J. Weber, J.W. Wald, Hj. Matzke, Mater. Lett. 3 (1985) 173.
[3] W.J. Weber, J.W. Wald, Hj. Matzke, J. Nucl. Mater. 138 (1986) 196.
[4] W.J. Weber, N.J. Hess, Nucl. Instrum. and Meth. B 80&81 (1993) 1245.
[5] S.X. Wang, B.D. Begg, L.M. Wang, R.C. Ewing, W.J. Weber, K.V. Govidan Kutty, J. Mater. Res. 14 (12) (1999) 4470.
[6] S.X. Wang, L.M. Wang, R.C. Ewing, K.V. Govindan Kutty, Mater. Res. Soc. Symp. Proc. 540 (1999) 355.
[7] S. Thevuthasan, C.H.F. Peden, M.H. Engelhard, D.R. Baer, G.S. Herman, W. Jiang, Y. Liang, W.J. Weber, Nucl. Instrum. and Meth. A 420 (1999) 81.
[8] M. Oueslati, M. Balkanski, P.K. Moon, H.L. Tuller, Mater. Res. Soc. Symp. Proc. 135 (1989) 199.
[9] B.D. Begg, W.J. Weber, R. Devanathan, J.P. Icenhower, S. Thevuthasan, B.P. McGrail, Environmental Issues and Waste Management Technologies in the Ceramic and Nuclear Industries V, Ceramic Transactions, vol. 107, American Ceramic Society, Westerville, OH, USA, 2000, p. 553.